

Synthesis of Br-doped TiO₂ hollow spheres with enhanced photocatalytic activity

Qianqian Wang · Shengli Zhu · Yanqin Liang ·
Zhenduo Cui · Xianjin Yang · Chunyong Liang ·
Akihisa Inoue

Received: 13 October 2016 / Accepted: 24 January 2017 / Published online: 16 February 2017
© Springer Science+Business Media Dordrecht 2017

Abstract The Br-doped hollow TiO₂ photocatalysts were prepared by a simple hydrothermal process on the carbon sphere template following with calcination at 400 °C. The structure and properties of photocatalysts were characterized by X-ray diffraction, Raman spectrum, scanning electron microscope, transmission electron microscopy, N₂ desorption–adsorption, UV–Vis spectroscopy, and X-ray photoelectron spectroscopy. The TiO₂ hollow spheres are in diameter of 500 nm with shell thickness of 50 nm. The shell is composed of small anatase nanoparticles with size of about 10 nm. The TiO₂ hollow spheres exhibit high crystalline and high surface area of 89.208 m²/g. With increasing content of Br doping, the band gap of TiO₂ hollow spheres

decreased from 2.85 to 1.75 eV. The formation of impurity band in the band gap would narrow the band gap and result in the red shift of absorption edge from 395 to 517 nm, which further enhances the photocatalytic activity. The appropriate Br doping improves the photocatalytic activity significantly. The TiO₂ hollow spheres with 1.55% Br doping (0.5Br-TiO₂) exhibit the highest photocatalytic activity under full light. More than 98% of RhB, MO, and MB can be photodegraded using 0.5Br-TiO₂ with concentration of 10 mg/L in 40, 30, and 30 min, respectively. The degradation rate of Br-doped photocatalysts was 40% faster than undoped ones.

Electronic supplementary material The online version of this article (doi:10.1007/s11051-017-3765-2) contains supplementary material, which is available to authorized users.

Keywords Bromine · Doped · TiO₂ · Hydrothermal method · Photocatalysis

Q. Wang · S. Zhu (✉) · Y. Liang · Z. Cui · X. Yang ·
A. Inoue
School of Materials Science and Engineering, Tianjin University,
Tianjin 300072, China
e-mail: slzhu@tju.edu.cn

S. Zhu · Y. Liang
Tianjin Key Laboratory of Composite and Functional Materials,
Tianjin 300072, China

C. Liang
Research Institute for Energy Equipment Materials, Hebei
University of Technology, Tianjin 300130, China

A. Inoue
Department of Physics, King Abdulaziz University, Jeddah 22254,
Saudi Arabia

Introduction

TiO₂ has caught increasing attentions as photocatalyst because of the increasing environment pollution (Hashimoto et al. 2005; Kumar and Devi 2011). However, wide applications were limited by its intrinsic drawbacks, such as difficulty of excitation due to wide band gap and easy recombination of the photogenerated electron–hole pairs (Froschl et al. 2012; Setvin et al. 2013). An effective strategy is additional components doping in TiO₂ to extending the photoresponse spectrum to the visible region (Irie et al. 2003; Klošek and Raftery 2001; Xu et al. 2002; Yu et al. 2002). Because of disadvantages of metallic doping, such as poor thermal

stability, photocorrosion, and serving as recombination centers (Song et al. 2015b; Zhang et al. 2011a), non-metallic doping (C, N, F, I, Br etc.) (Burda et al. 2003; Ohno et al. 2003; Wang and Lewis 2006) was paid more attentions in recent years. Among the non-metallic doping, halogen doping attracted many interests because it could shift the photo response region to the visible light range (Hong et al. 2005; Zhou et al. 2008). Compared to the F and I doping, the Br doping could result in narrower band gap. For example, the band gap of Br, Cl co-doped TiO₂ is 2.85 eV (Luo et al. 2004) and the Br, N co-doped TiO₂ shifts from 400 to 475 nm (Shen et al. 2009), while the band gap of I-doped TiO₂ is 3.03 eV (Zhang et al. 2011b). However, Br is difficult to dope in the oxide because of the large radius. The researches on Br-doped TiO₂ are limited, and most of which are co-doped with other elements. Sheng et al. (2008) reported that the Br, N co-doped TiO₂ could enlarge the absorptance to the visible light region. The possible mechanism was that the existence of Br transformed Ti(IV) into Ti(III), furthermore restrain the recombination of photogenerated electrons and holes. Gao et al. (2008) prepared Br and Sm co-doped TiO₂ by an improved sol-gel method. The absorption edge of Br and Sm co-doped TiO₂ is longer than 400 nm. The probable reason is that the surface oxygen vacancy (SOV) and defects lead to the increase amount of oxygen vacancies in the TiO₂. However, the above researches focused on co-doped TiO₂. The effect of single Br doping is still unclear and needs further investigation.

Morphologies of photocatalysts can influence the photocatalytic efficiency (Lou et al. 2008; Xu et al. 2009; Yu and Kudo 2006). The hollow microsphere structure attracted many attentions because of many advantages, such as low density, high surface area, good surface permeability, and high light-harvesting efficiencies (Yu et al. 2007). Fe-doped WO₃ hollow nanostructures were synthesized by a template method (Song et al. 2015b). These Fe-doped WO₃ hollow spheres have high surface area and superior visible-light-driven photocatalytic activity. The band gap of the Fe-doped WO₃ is facilely tunable by controlling the Fe-doped contents. In addition, a kind of excellent visible light responsive C, N co-doped TiO₂ hollow spheres was prepared using carbon spheres as template (Ao et al. 2009). The major difficulty is to maintain the hollow sphere structure during the removal of templates. In addition, the hollow spheres are composed of lots of nanoparticles. The size of nanoparticles could determine the diffusion length for

photogenerated electrons and holes. The smaller ones can restrain the recombination of photogenerated electrons and holes. Therefore, the stable method to prepare hollow spheres composed of small nanoparticles is worth to be investigated.

In the present paper, single Br-doped TiO₂ hollow spheres composed of small nanoparticles were successfully synthesized through a hydrothermal method with the carbon spheres as template. The photocatalytic properties were evaluated by degrading rhodamine B (RhB), methyl orange (MO), and methyl blue (MB).

Experimental

Preparation of carbon spheres

The carbon spheres were made by the hydrothermal method according to Ref. (Sun and Li 2004). Uniform glucose solution of 35 ml (C₆H₁₂O₆) at concentration of 0.5 mol/l was transferred to a Teflon vessel and treated hydrothermally at 180 °C for 8 h. The as-formed black products were washed and centrifuged with abundant deionized water, followed by drying in the oven at 50 °C for 8 h.

Preparation of Br-TiO₂ hollow spheres

All chemicals used in this experiment were of analytical purity (AR) without further purification. The ammonium bromide (NH₄Br) was dissolved evenly in the solution mixed by 20 ml of *N,N*-dimethylformamide (DMF) and 20 ml of anhydrous ethanol (C₂H₅OH). The as-prepared carbon spheres (0.2 g) were dispersed to the above-mentioned solution by sonication stirring for 30 min. Then, the tetrabutyl titanate (TBOT, 4 mmol) was added dropwise into the above solution with 2-h continuous stirring at room temperature. After stirring, the final black mixture was transferred to a Teflon-lined vessel, followed by hydrothermal treatment at 150 °C for 12 h. The precipitate in the Teflon-lined vessel was taken out, centrifuged, cleaned with distilled water and ethanol for three times, and then dried in an oven in air at 50 °C for 8 h. Finally, the Br-doped TiO₂ hollow spheres were gained by annealing the products in the chamber furnace at 400 °C for 6 h (Song et al. 2015b).

The Br concentration in Br-doped TiO₂ nanostructures was controlled by the mole ratio of NH₄Br and TBOT in the solution. The real ratios

of Br (At %)/Ti (At %) were 0, 1.14, 1.55, 1.87, and 2.33% (Table 1, data from the EDX) by mole percentage for the $\text{NH}_4\text{Br}/\text{TBOT}$ ratio of 0:4, 1:4, 2:4, 3:4, and 4:4, respectively. The samples were denoted in the way of “ $x\text{Br-TiO}_2$ ”, where x is the nominal mole percentage of Br relative to TBOT. For example, 0.5Br-TiO_2 represents 2 mmol Br-doped 4 mmol TBOT. In order to compare, the undoped TiO_2 was prepared following the equal procedure. All samples were milled before characterization, electrochemical experiment, and photocatalysis experiments.

Material characterization

The morphology and crystal structure were characterized by transmission electron microscopy (TEM, Philips Tecnai G2 F20) and scanning electron microscope (FE-SEM, Hitachi S-4800) which was equipped with an energy-dispersive X-ray (EDX) spectrometer. The X-ray diffraction (XRD, RIGAKU/DMAX) was used to examine the crystal structure of the samples. X-ray photoelectron spectroscopy (XPS, PHL1600ESCA) was employed to analyze the surface chemicals. The Raman spectra were gathered by the DXR Microscope (Thermo Electron Corporation) with the excitation wavelength of 532 nm. Nitrogen adsorption isotherms of the samples were measured using an autosorb iQ instrument (Quantachrome, USA). The powder samples pretreat at 150 °C for 24 h to remove the water. The total surface was calculated from the Brunauer–Emmett–Teller (BET) method, and the pore size distribution data was calculated using the Barrett–Joyner–Halenda (BJH) method based on the adsorption and desorption data. Diffuse reflection spectra and optical properties were collected on a Shimadzu (UV-2700) UV–Vis spectrophotometer.

Photocatalytic experiments

The photocatalytic activity of the series of samples for the degradation of organic contaminants was evaluated by the RhB, MO, and MB under the light. Each test was repeated 5 times. Then, the degradation of RhB, MO, and MB was characterized by the intensity of the corresponding characteristic absorption peaks at the wavelengths of 553, 463, and 598 nm. The degradation rate is calculated by C/C_0 . C represents the intensity of absorption peaks at the wavelengths of 553, 463, and 598 nm. C_0 represents the intensity of absorption peaks after the dark adsorption reaction. Twenty-milligram catalysts were suspended in a 50 ml of RhB, MO, and MB aqueous solution (10 mg/l). The solution was stirred for 30 min in the dark. The absorption reaction equilibrium curves are shown in Fig. s1. The absorption equilibriums were obtained after 30-min dark absorption reaction with the existence of photocatalysts. It can be observed that the absorption of dye RhB and MO is little, while the absorption of dye MB is much higher. A 500-W Xenon lamp was served as the light source with the light intensity of 110 mW/cm^2 . The liquid is sampled by 3 ml at a break of 10 min and put back where it comes from after measurement. The system was open to the air, maintaining the room temperature by cold water bath. The test was carried out on a Shimadzu (UV-2700) UV–Vis spectrophotometer.

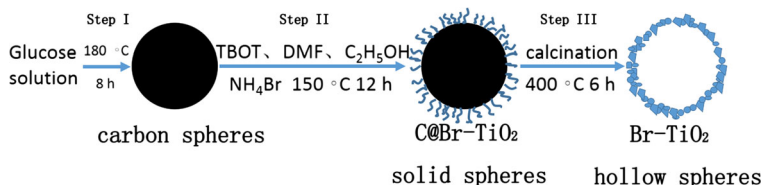
Results and discussion

The Br-doped TiO_2 nanostructures were prepared using carbon spheres as hard templates. The syntheses were schematically illustrated in Fig. 1. In step II, the TBOT hydrolyze rapidly, complying with double molecular nucleophilic substitution reaction, with the small

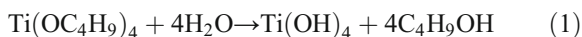
Table 1 Physicochemical properties and photocatalytic performances of as-prepared samples

Samples	Theory ratio of Br/Ti	O At%	Br At%	Ti At%	Actual ratio of Br/Ti %	Raman shift (cm^{-1})	E_g (eV)	Photocurrent density (mA/cm^2)
TiO_2	0:4	74.1	/	25.9	0	152.15	2.85	0.0305
0.25Br-TiO_2	1:4	62.81	0.42	36.76	1.14	152.62	2.67	0.0342
0.5Br-TiO_2	2:4	71.13	0.44	28.43	1.55	154.88	2.65	0.0357
0.75Br-TiO_2	3:4	69.49	0.56	29.95	1.87	156.82	2.64	0.0314
1.0Br-TiO_2	4:4	72.77	0.62	26.61	2.33	158.67	1.75	0.0191

Fig. 1 The synthesis of the Br-doped TiO₂ hollow spheres



amounts of H₂O in the anhydrous ethanol (C₂H₅OH). The reaction is as follows:



Then, the polycondensation occurs. The final products of hydrolysis reaction and polycondensation are TiO₂·nH₂O. TiO₂ crystal nucleus and Br⁻ could be homogeneously absorbed on the surface of carbon spheres because there are lots of -OH and -C=O groups on carbon spheres' surface (Sun and Li 2004). The solution is weak acid solution because of the existence of NH₄Br. The environment with low pH can increase the length to diameter ratio of anatase TiO₂ (Dai et al. 2009). Therefore, the nanowires grow on the carbon spheres evenly. In step III, the Br-doped TiO₂ hollow nanospheres could be formed through ablation of carbon in the C@Br-TiO₂ core shell nanostructure by calcination in air at 400 °C for 6 h. The diameter of hollow spheres decreases due to the shrink after the ablation of carbon spheres. The nanowires transform to the nanoparticles based on the principle of minimum energy. The calcination temperature is an important factor in the synthesis of Br-doped TiO₂ hollow spheres. If the calcination temperature is too low, carbon sphere templates are difficult to remove. Contrarily, the anatase TiO₂ may convert to rutile TiO₂ when temperature is too high (Wetchakun and Phanichphant 2008). According to the thermogravimetric (TG) results (as shown in Fig. S2), the calcination temperature was chosen as 400 °C.

Figure 2 shows the XRD patterns of TiO₂ samples doped with different concentrations of Br. The pattern of sample without Br-doping is readily in agreement with anatase TiO₂. With the increasing Br contents, no other obvious peak is detected, indicating that the Br concentrations in the TiO₂ would be very low (Song et al. 2015a; Zhang et al. 2012). In addition, the atom radii of Br (0.045 nm) and Ti (0.054 nm) are similar. Thus, the Br could be doped into the crystal lattice of TiO₂ with little lattice distortion. The peak of (101) slightly shifts to right, and the intensity of the peaks decreases gradually with increasing Br content (inset in Fig. 2).

This may be attributed to the substitute of relative smaller Br for Ti, which can also be proved by XPS results below. The doping of Br caused the lattice distortion, and then reduced the interplanar spacing.

The Raman spectrum is shown in Fig. 3. Pure TiO₂ only contains the characteristic peaks of the anatase phase, which is in agreement with the result of XRD. The peaks at 152, 407, 527, and 648 cm⁻¹ are ascribed to the four Raman-active modes of anatase phase with the symmetries of Eg, B1g, B2g, and Eg, respectively (Toshiaki Ohsaka and Fujiki 1978). With Br doping, no other peaks could be observed. Remarkably, the characteristic peaks of the samples exhibit blue shift and intensity decreasing gradually with increasing Br content (inset in Fig. 3 and data in the Table 1), as a result of Br occupying the substitutional site in TiO₂ and causing lattice distortion (Li et al. 2015).

Figure 4a shows SEM image of the carbon sphere template. The carbon spheres exhibit smooth surface and uniform diameter of about 500 nm. After hydrothermal reaction, some nanowires grow evenly on the surface of carbon sphere template. Accordingly, the diameter of microspheres increases to about 600 nm. After the calcination at 400 °C, both the shape and dimension of these microspheres are kept well (as shown in inserted images of Fig. 4b-f), illustrating that the

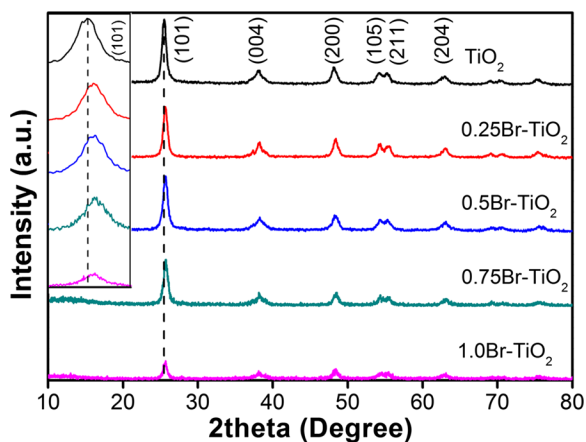


Fig. 2 XRD patterns of the as-prepared samples; inset is the partial enlarged detail of (101) peaks

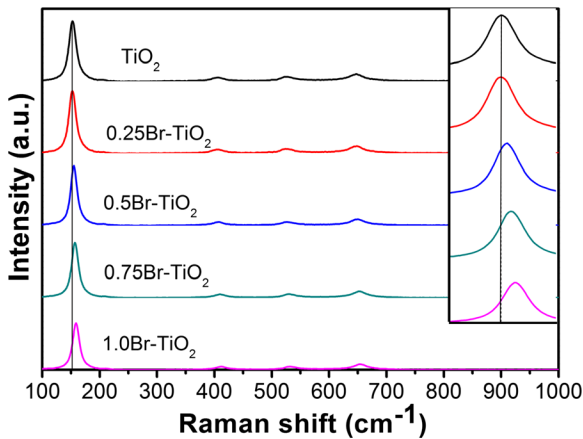


Fig. 3 Raman spectra of the as-prepared samples; *inset* is the partial enlarged detail of main peaks

thermal decomposition of carbon spheres would not break the shell structure of the TiO_2 . In addition, the nanowires on the surface of carbon spheres (Fig. s3) transformed to the nanoparticles. The possible reason is that the structures of nanowires are loose on the surface of carbon spheres and the nanoparticles have the smaller surface energy than the nanowires. During calcinations at 400 °C, the carbon spheres disappear gradually and

the crystals of TiO_2 grow little by little. The nanoparticles unite closely due to the strong interaction between each other. Then, the samples can retain the hollow sphere structure after the disappearance of carbon spheres.

The internal microstructure of these hollow microspheres was further investigated through TEM. Fig. 5a shows morphology of the bare carbon spheres with the diameter of 500 nm. The C@TiO_2 (Fig. 5c) and C@Br-TiO_2 (Fig. 5e, g and Fig. s4a, c) are solid spheres due to the inner templates of carbon spheres. After the calcination treatment, the solid spheres transformed to the hollow spheres (Fig. 5d, f, h and Fig. s4b, d) with the diameter of about 500 nm and shell thickness of about 50 nm, indicating the decomposition of carbon sphere template. So, we can observe that the spheres shrunk after calcination treatment. The HRTEM reveals that the Br-TiO_2 on the surface of carbon spheres had the morphology of nanowires (as shown in the inserted image in Fig. 5g) with the total diameter of 600 nm. However, after annealing, the nanowires Br-TiO_2 shells transformed to nanoparticles with average diameter of 10 nm (as shown in Fig. 5b). The change from nanowires to the nanoparticles is in accord with the SEM

Fig. 4 SEM images of **a** carbon spheres, **b** C@TiO_2 , **c** C@0.25Br-TiO_2 , **d** C@0.5Br-TiO_2 , **e** C@0.75Br-TiO_2 , and **f** 1.0Br-TiO_2 . The inserted images are the hollow morphologies of above products after calcinations

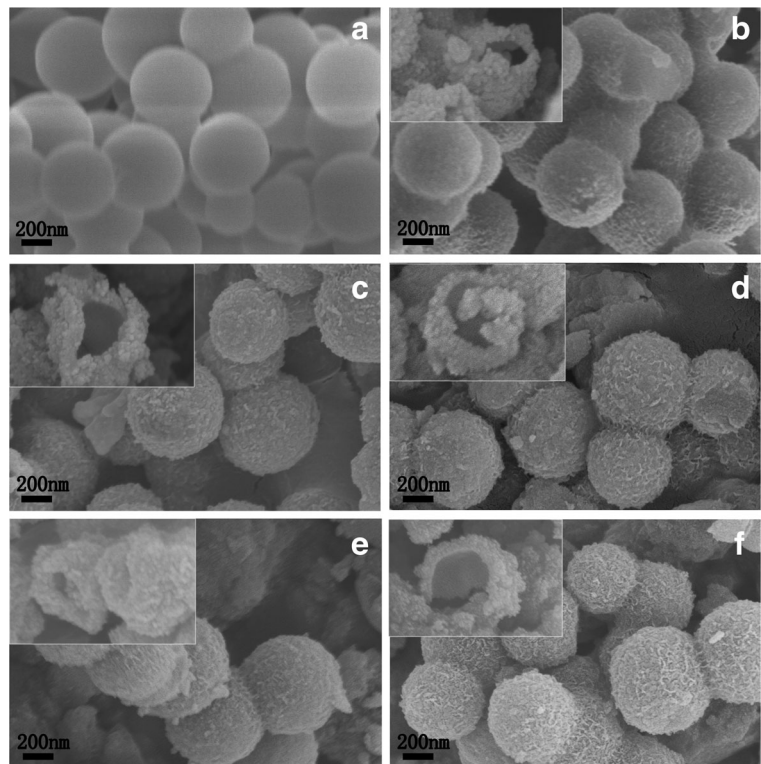
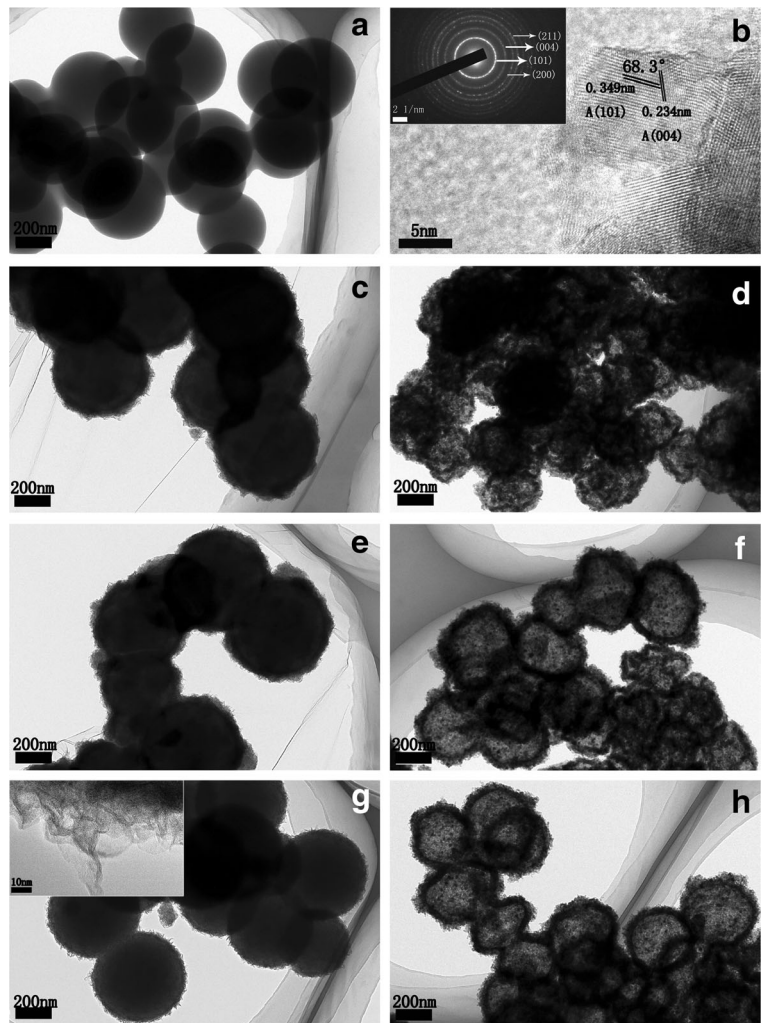


Fig. 5 TEM images of **a** carbon spheres, **c** C@TiO₂, **d** TiO₂, **e** C@0.25Br-TiO₂, **f** 0.25Br-TiO₂, **g** C@0.5Br-TiO₂, and **h** 0.5Br-TiO₂. **b** HRTEM image of the 0.5Br-TiO₂ and SAED (inserted). Inset image in **g** is the HRTEM of C@0.5Br-TiO₂ sphere surface



results. The lattice spacings of 0.349, 0.234, and the angle (68.3°) correspond to the (101), (004) lattice planes and their theoretical angle of anatase TiO₂, respectively. The lattice spacing has an obvious shrinkage relative to the theoretical value of 0.352 and 0.238 nm, proving the substitute of Ti sites by Br. The selected area electron diffraction (SAED) result (as shown in inset of Fig. 5b) also confirmed the existence of the anatase phase. EDX mapping further exposes the hollow sphere structure of the Br-TiO₂ hollow spheres (Fig. 6). It is noticeable that a small quantity of Br is found in the region of the TiO₂ shell, confirming that the TiO₂ is doped by Br successfully.

Through the calcination, the carbon sphere template was decomposed to the CO₂ (Shen et al. 2005; Wang et al. 2007), leading to the hollow spheres. Figure 7

demonstrates the BET results, revealing type IV physisorption isotherms according to the IUPAC recommendations (Dinkar et al. 2016). The hysteresis loops indicate the typical mesoporous materials. The specific areas of C@Br-TiO₂ and Br-TiO₂ are 170.2 and 89.2 m²/g, respectively. In general, the specific surface area of hollow spheres should be higher than the solid one. But in our case, the specific areas decreased after annealing. The probable reason is that the surface of C@0.5Br-TiO₂ is composed of nanowires, while 0.5Br-TiO₂ is composed of nanoparticles. The inset images of Fig. 7 reveal that the sizes of most pores of C@Br-TiO₂ and Br-TiO₂ are about 3 and 7 nm, respectively. The BET surface area of TiO₂ is strongly influenced by the morphologies. In some papers, the BET surface area of TiO₂ was measured as 199.8 m²/g (nanoparticles), 51.1 m²/g (commercial P25) (Xu et al.

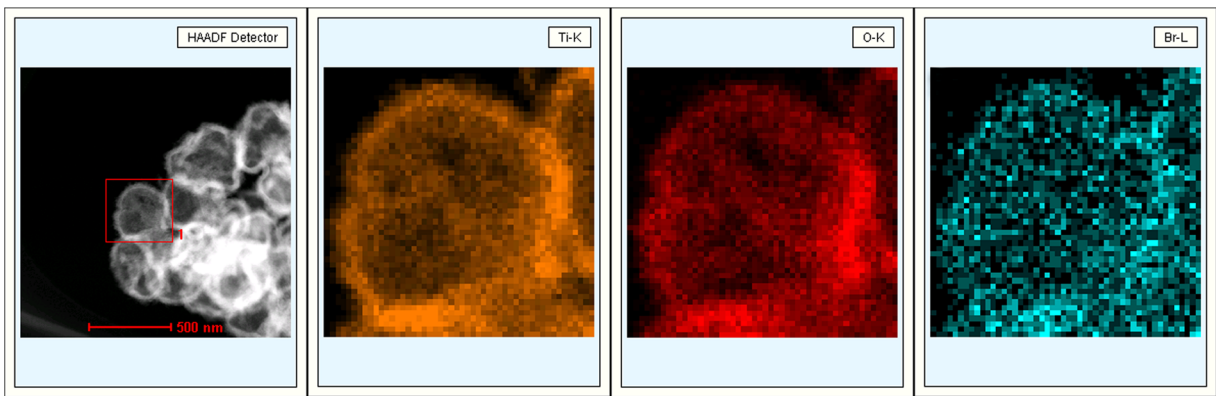


Fig. 6 STEM image and corresponding EDX elemental mapping of Ti-K, O-K, and Br-L of 0.5Br-TiO₂

2014), 146.4 m²/g (nanoparticles) (Zhang et al. 2012), and 57.1 m²/g (nanosheets) (Xu et al. 2013), respectively. The surface area in our case (89.2 m²/g) is in the medium level. In addition, this surface area is higher than other hollow spheres with the alike diameter mentioned by other references (Deng et al. 2008; Yu et al. 2009; Zhang et al. 2015).

The UV–Vis diffuse reflectance spectra of undoped TiO₂ and Br-doped TiO₂ samples are shown in Fig. 8. The absorption edge of 1.0Br-TiO₂ hollow spheres is around 517 nm, which is higher than that of the undoped TiO₂. The absorption is extended to the visible light region. The inset image of Fig. 8 illustrates the band gap values for the calculation of indirect transition, which is obtained by the junction of extension cord and abscissa (listed in Table 1). With Br doping, the band gaps of as-prepared photocatalysts decrease and the visible light responses increase. The 1.0Br-TiO₂ has the smallest band gap and largest visible light absorbance. The undoped TiO₂ has a band gap of 2.85 eV, while the band gaps decrease to around 1.75 eV (1.0Br-

TiO₂) with the increasing contents of Br doping. The reason is that the Br doping introduces the impurity level between the conduction band and valence band (Kesong Yang et al. 2009; Asahi et al. 2001), promoting the transition of electron and then narrowing the band gap.

Figure 9 shows XPS spectrum of 0.5Br-TiO₂, which indicates the existence of Ti, Br, and O elements. The existence of the Br element in the hollow TiO₂ spheres is proved in Fig. 9a (the elemental analysis results are shown in inset of Fig. 9a). The molar ratio of Br/Ti is 1.64%, in keeping with the EDX data (1.55%, Table 1). As shown in Fig. 9b, the XPS spectrum of Ti 2p orbit exhibits doublet located at 459.0 eV (Ti 2p_{3/2}) and 464.7 eV (Ti_{2p1/2}), respectively. Both of peaks correspond to Ti⁴⁺. The XPS spectrum of Br 3d orbit (Fig. 9c) shows double peaks around 68.0 eV (Br 3d_{5/2}) and 69.0 eV (Br 3d_{3/2}), in which locations are higher than the results in some papers (Escard et al. 2002; Kamada et al. 1992; Kamada et al. 1993). Through the theoretical calculation of Yang et al. (2008b), Br substitute for Ti

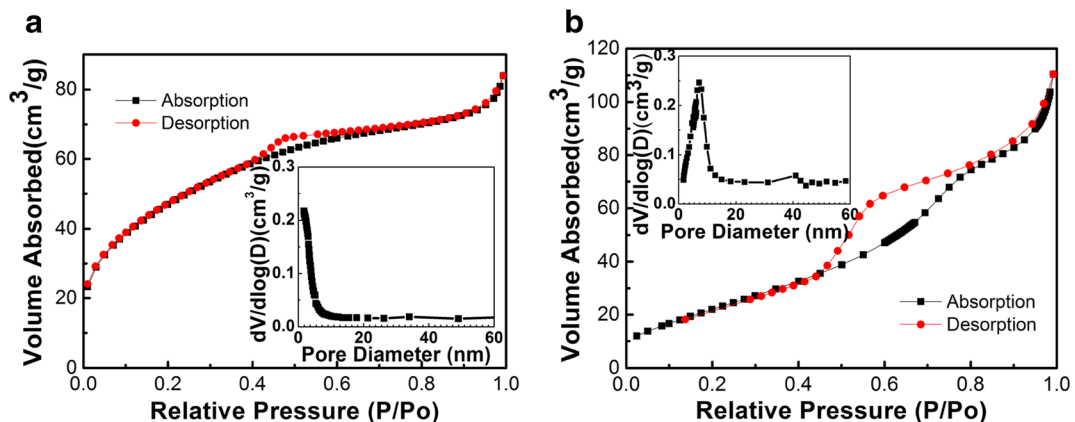


Fig. 7 N₂ adsorption/desorption isotherms and pore size distribution of **a** C@0.5Br-TiO₂ and **b** 0.5Br-TiO₂ hollow spheres

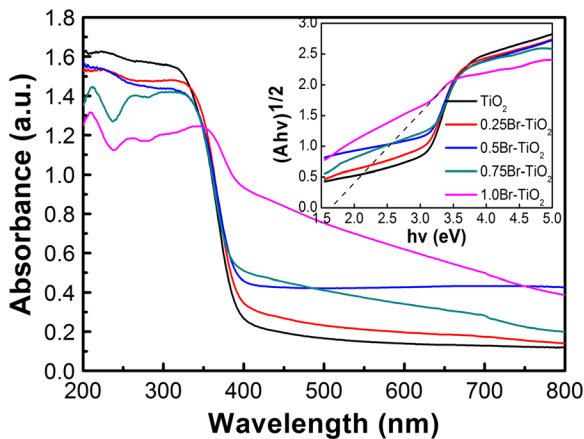


Fig. 8 UV-Vis absorption spectra of undoped TiO₂, 0.25Br-TiO₂, 0.5Br-TiO₂, 0.75Br-TiO₂, and 1.0Br-TiO₂ catalysts from 200 to 800 nm, *inset* being the spectra after conversion (absorbance was converted to $(A\cdot hv)^{1/2}$ values, then plot relative to the horizontal $h\nu$ (eV))

site is easier than that for O site in O-rich environment. For Br substitute for Ti site, Br atom presents as Br⁴⁺ (s^2p^1) ions. Singly occupied band state is made up of Br

4p, which appears in the band gap of TiO₂. The possible way for the formation of Br⁴⁺ is as follows: Br⁻ ions in the precursor solution could be oxidized by the h^+ to Br⁵⁺ firstly, and then, Br⁵⁺ ions were doped in the Ti site and change to the Br⁴⁺ by the influence of surrounding clouds finally. Br-doped TiO₂ has a pronounced band gap narrowing (about 0.2 eV) through the theoretical calculation. This phenomenon is in agreement with my own data (0.2 eV, Table 1). Br⁴⁺ ions substitute for Ti⁴⁺ are present in the Br–O–Ti bond (Kuo and Hsiao 2015; Liu et al. 2009). The XPS spectrum of the O 1s orbit (Fig. 9d) shows a wide peak, which is fitted with four peaks. The peak at around 529.6 and 530.5 eV can correspond to lattice oxygen Ti–O–Br and Ti–O–Ti. Other peaks around 531.4 and 532.5 eV can be attributed to surface hydroxyl groups (Liu et al. 2009; Tojo et al. 2008) and chemisorbed oxygen on the surface (Liu et al. 2006; Zhou et al. 2008).

Figure 10 shows the photocatalytic performance by degradation of the RhB, MO, and MB. As shown in Fig. 10a, RhB has little degradation under illumination

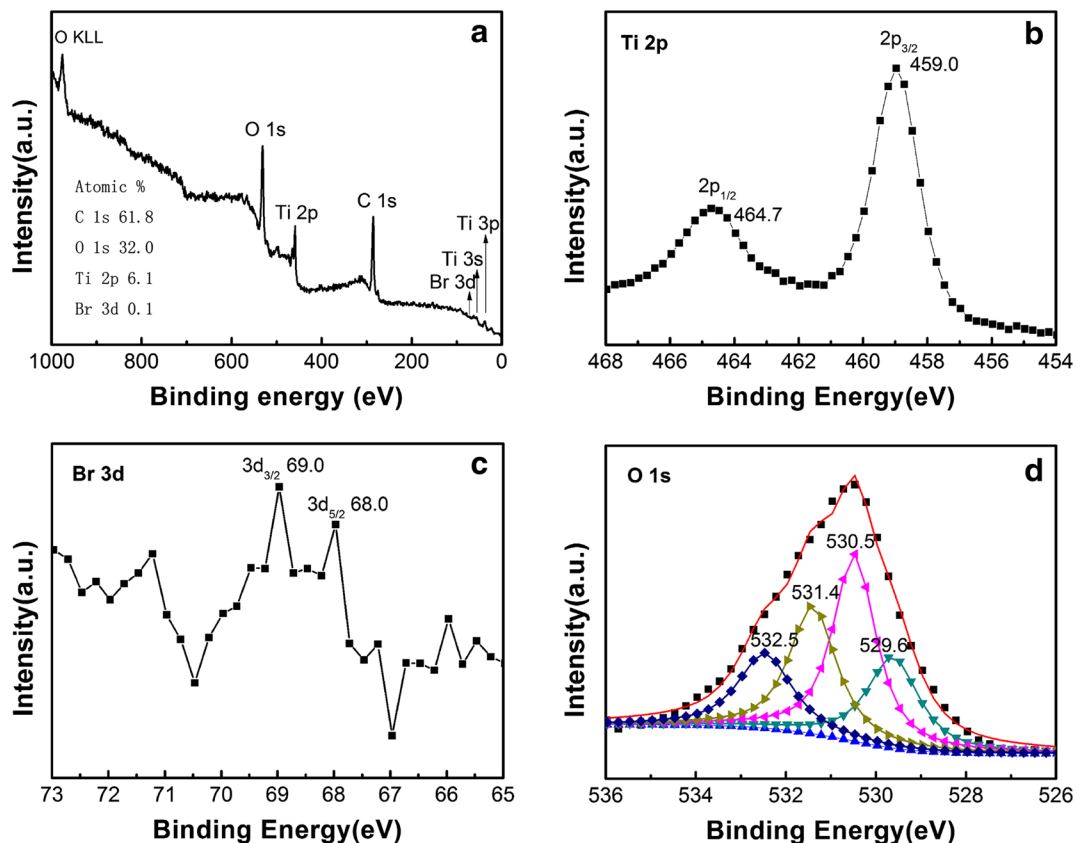


Fig. 9 XPS spectra of 0.5Br-TiO₂ for **a** an overview spectrum, **b** Ti2p spectrum, **c** Br3d spectrum, and **d** O1s spectrum

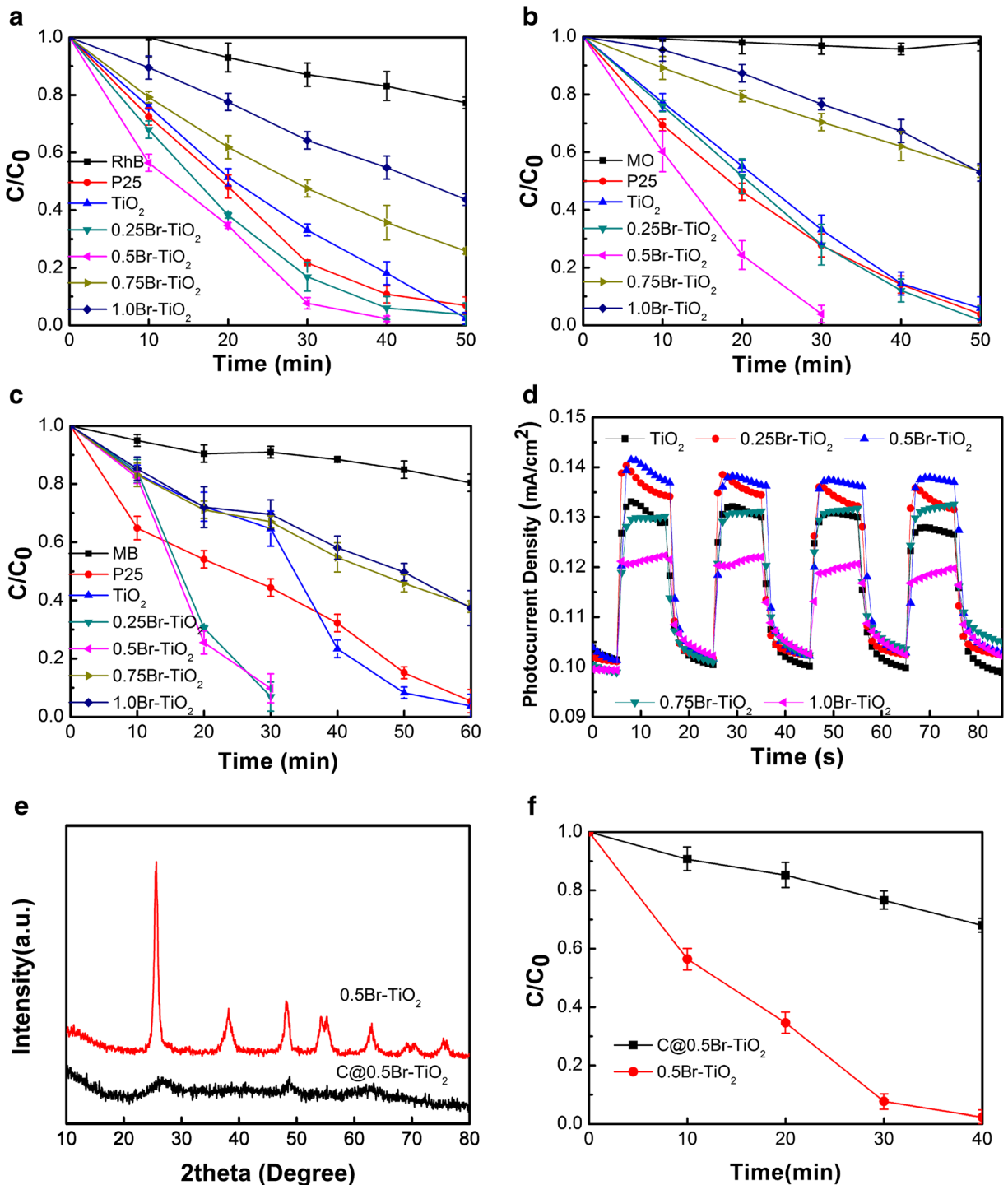


Fig. 10 a Photodegradation of RhB, b photodegradation of MO, c photodegradation of MB, d the photocurrent density of the as-prepared products, e XRD of C@0.5Br- TiO_2 and 0.5Br- TiO_2 , f photodegradation of RhB with C@0.5Br- TiO_2 and 0.5Br- TiO_2

without any catalyst. The pure TiO_2 hollow spheres possess certain photocatalytic efficiency due to the large band

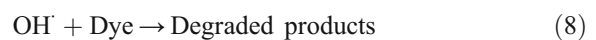
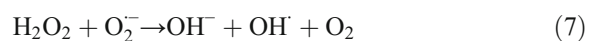
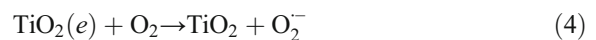
gap of 2.85 eV (Table 1). The Br-doped TiO_2 hollow spheres with appropriate Br content exhibit enhanced

photocatalytic activity. The degradation of RhB by the Br-doped TiO₂ with appropriate Br content is faster than the commercial P25 and undoped TiO₂. With the increasing concentration of Br doping, the photocatalytic activity increases firstly, then decreases. The 0.5Br-TiO₂ exhibited the best photocatalytic performance. For 0.5Br-TiO₂ sample, the characteristic absorption peak of RhB (about 553 nm) (Wu et al. 2012; Zhao et al. 2011) vanishes gradually and completely disappears after 40-min continuous illumination, while 50 min for the undoped TiO₂. The degradation rate of 0.5Br-TiO₂ was 20% faster than undoped ones. The decreasing of photocatalytic activity for the 0.75Br-TiO₂ and 1.0Br-TiO₂ may be due to the easy combination of photogenerated electrons and holes. Figure 10b, c show the photodegradation curves of MO and MB for the series of TiO₂ with different Br contents. The results exhibit similar tendency with the photodegradation of the RhB: with the increasing of Br contents, the photodegradation efficiency increases first, then decreases. The photocatalytic activities of Br-doped TiO₂ hollow spheres with appropriate Br content are improved. About 96% of MO and 99% of MB were degraded in 30 min in the case of 0.5Br-doped TiO₂. The degradation rate of 0.5Br-doped TiO₂ photocatalysts was 40% faster than undoped ones. However, the degradation of MB is faster than RhB and MO due to the higher absorption of MB by photocatalyst (as shown in Fig. s1).

Photocurrent intensity is regarded as an effective parameter to evaluate the photocatalytic performance, which is generally believed that the greater the photocurrent intensity, the higher the efficiency of formation and separation for holes and electrons (Liu et al. 2012). The photocurrent value became zero when the light turned off, while the photocurrent value reestablish soon when light on. The stable photocurrents of undoped TiO₂, 0.25Br-TiO₂, 0.5Br-TiO₂, 0.75Br-TiO₂, and 1.0Br-TiO₂ are 0.0305, 0.0342, 0.0357, 0.0314, and 0.0191 mA/cm², respectively (Table 1). With the increasing Br content, the photocurrent density (Fig. 10d) increases firstly, then decreases. 0.5Br-TiO₂ exhibits the highest photocurrent density. The decreasing photocurrent density for 0.75Br-TiO₂ and 1.0Br-TiO₂ is due to the low rate for separation of holes and electrons, corresponding with the decreasing photocatalytic performance. The reason is that the too much doped Br would mainly act as recombination centers to decrease the photocatalytic efficiency. The response of the photocurrent maintains a high repeatability after many cycles. When the doping concentration ratio is 1.55% (0.5Br-TiO₂), the efficiency increases by about 17% compared with the

undoped TiO₂ because of more electron generation and higher separation efficiency (Cummings et al. 2012).

The mechanism of photocatalytic degradation of dye is shown in Fig. s5. A series of reactions could occur during the photocatalytic degradation of organic dyes, as shown in Eqs. (2)–(9) (Arabzadeh and Salimi 2016). The surface of photocatalysts produces electrons and holes with the illumination (Eq. (2)), then further forms the hydroxyl free radicals and superoxide radical oxygen anion (Eqs. (3) and (4)). In the following, the superoxide radical anion O₂^{•-} could transform to hydroxyl radical OH[•] through 3 continues reactions (Eq. (5)–(7)). It is well known that the OH[•] radical is a powerful oxidizing agent capable of degrading most dyes (Eq. (8)). Also, photo-generated holes can degrade the organic dyes to CO₂, H₂O, and inorganics (Eq. (9)).



To explain the increased photocatalysis activity of Br-doped TiO₂, three reasons are proposed. First, Br⁻ ions in the precursor solution could be oxidized by the h⁺ to Br⁵⁺. The Br⁵⁺ ions dope in the Ti site and change to the Br⁴⁺ by the influence of surrounding clouds. Since the doping Br⁴⁺ for Ti⁴⁺ ions in the crystal lattice of TiO₂ could create a new impurity level above the original valence band of TiO₂ (Yang et al. 2008b), the electrons are easier to be promoted to the conduction band from the impurity level, which could increase the absorption

intensity in range of visible light and improve the photocatalytic performance. Second, if the Br concentration is lower than its optimal molar ratio, Br^{4+} ions would be mainly doped in the surface of the samples (Song et al. 2015b), which could be proved by the approximation of XPS data and EDX data. Br^{4+} ions could trap and transfer electrons and holes to inhibit the recombination of photogenerated holes and photogenerated electrons (Tong et al. 2008). This reason is more important than the narrow band gap and more electron generation. Thirdly, the existence of reactive {001} facets (proved by HRTEM) can improve the photocatalytic performance (Liu et al. 2010; Wetchakun and Phanichphant 2008). The doping of Br has some beneficial effect on the percentage of {001} facets relative to all facets (Yang et al. 2008a).

Morphology and crystallinity of photocatalysts also influence the photocatalytic efficiency. $\text{C}@0.5\text{Br-TiO}_2$ and 0.5Br-TiO_2 samples are selected to investigate the influence of morphologies and crystallinity. Figure 10e shows the XRD pattern of $\text{C}@0.5\text{Br-TiO}_2$ and 0.5Br-TiO_2 samples. It is obvious that the crystalline of $\text{C}@0.5\text{Br-TiO}_2$ is weaker than the 0.5Br-TiO_2 because of the calcination at 400°C . The little peaks can be observed clearly of $\text{C}@0.5\text{Br-TiO}_2$, in keeping with the anatase phase. The $\text{C}@0.5\text{Br-TiO}_2$ is the mixture of amorphous state and crystalline state. The calcination of $\text{C}@0.5\text{Br-TiO}_2$ leads to the increases of crystalline. Generally, the photocatalysts with carbon have a good adsorption performance. The adsorption of dye RhB by the $\text{C}@0.5\text{Br-TiO}_2$ (Fig. s6) is much higher than that by the 0.5Br-TiO_2 . Figure 10f reveals that the 0.5Br-TiO_2 hollow spheres have a higher photocatalysis performance than the $\text{C}@0.5\text{Br-TiO}_2$ solid spheres. The reasons are as follows. The crystallinity of 0.5Br-TiO_2 is higher than the $\text{C}@0.5\text{Br-TiO}_2$. Although the adsorption of dye in the dark has the opposite rule, it is not the main influence factor. The electronic migration in the photocatalyst is the key factor of photocatalytic efficiency. The hollow spheres have the shorter distance than the solid ones at the same diameter. In addition, the hollow spheres have good surface permeability (Yu et al. 2007), which is helpful to the mass transfer. Hence, the hollow spheres exhibit higher photocatalytic activity.

As mentioned above, there are many factors which could influence the photocatalytic activity, such as lower Eg, more electron generation, higher separation efficiency, appropriate morphology, and crystallinity. The lower Eg would lead to more electron generation. Compared

to the more electron generation and lower band gap, higher separation efficiency is considered as more essential factor for the photocatalytic performance. Figure 10d shows the decreasing photocurrent density for the 0.75Br-TiO_2 and 1.0Br-TiO_2 samples due to the relative lower separation rate of holes and electrons,

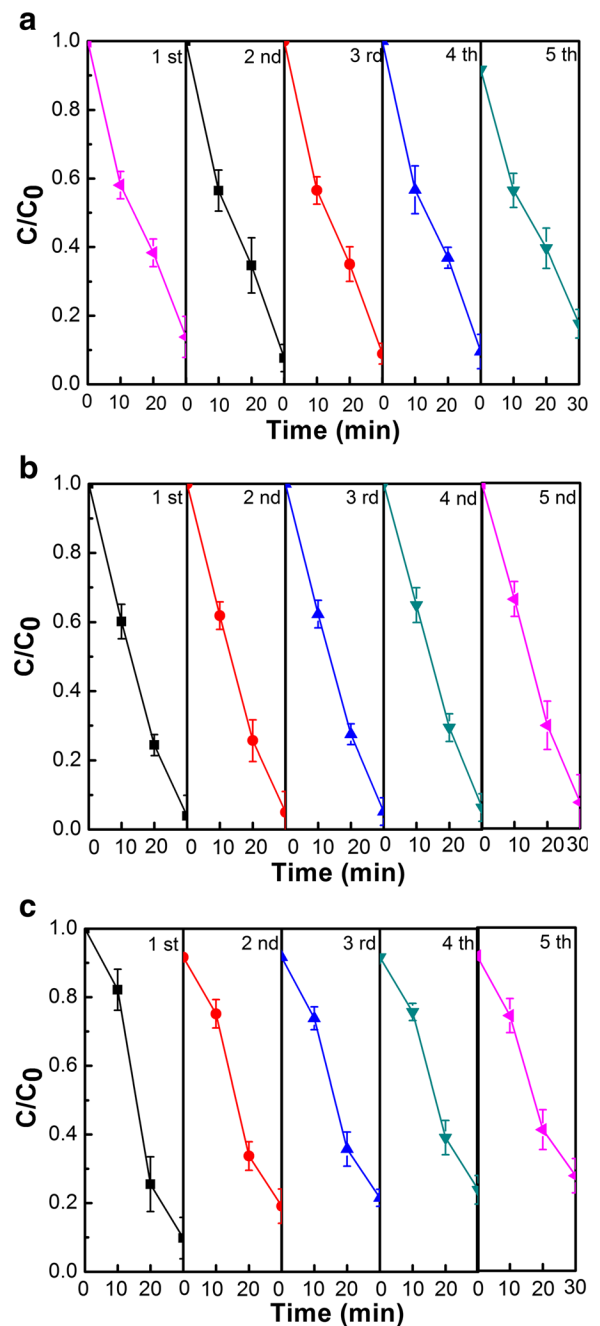


Fig. 11 Five cycles of photodegradation of **a** RhB, **b** MO, and **c** MB using 0.5Br-TiO_2

even though these two samples exhibit lower E_g . The morphology and crystallinity influence the photocatalytic properties from different aspects, which are considered as similar importance as the separation efficiency.

We have studied the stability of the photocatalyst 0.5Br-TiO₂ by collecting, reusing, and testing the same photocatalyst for 5 cycles (Fig. 11). There was just a small loss in photocatalytic activity. This may be caused by the incomplete collection during cycling. In short, the as-prepared photocatalysts show excellent stabilities.

Conclusions

In conclusion, we have successfully prepared the Br-doped TiO₂ hollow spheres with the diameter of about 500 nm and shell thickness of about 50 nm by using a template hydrothermal method. The Br atoms were doped in the as-prepared hollow TiO₂ lattice. The band gap of the Br-doped TiO₂ could decrease to 1.75 eV. The light response region is broadened to the visible-light region due to the formation of impurity bands in the band gap. The Br-doped TiO₂ hollow spheres exhibit the highest photocatalytic activity under full light for 1.55% Br doping ratio. This research provides a simple and effective method to synthesize Br-doped hollow TiO₂ spheres with enhanced photocatalytic performance.

Compliance with ethical standards

Funding This study was funded by the National Natural Science Foundation of China (51172159), Recruitment Program of Global Experts “1000 Talents Plan” of China (WQ20121200052), and Key Project of Natural Science Foundation of Tianjin City (14JCZDJC38600).

Conflict of interest The authors declare that they have no conflict of interest.

References

- Ao Y, Xu J, Fu D, Yuan C (2009) Visible-light responsive C,N-codoped titania hollow spheres for X-3B dye photodegradation. *Micropor Mesopor Mat* 118:382–386. doi:10.1016/j.micromeso.2008.09.010
- Arabzadeh A, Salimi A (2016) One dimensional CdS nanowire@TiO₂ nanoparticles core-shell as high performance photocatalyst for fast degradation of dye pollutants under visible and sunlight irradiation. *J Colloid Interface Sci* 479:43–54
- Asahi R, TM T, Ohwaki K, Taga AY (2001) Visible-light photocatalysis in nitrogen-doped titanium oxides. *Science* 293:269–271
- Burda C, Lou YB, Chen XB, Samia ACS, Stout J, Gole JL (2003) Enhanced nitrogen doping in TiO₂ nanoparticles. *Nano Lett* 3:1049–1051
- Cummings CY, Marken F, Peter LM, Tahir AA, Wijayantha KGU (2012) Kinetics and mechanism of light-driven oxygen evolution at thin film alpha-Fe₂O₃ electrodes. *Chem Commun* 48:2027–2029
- Dai Y, Cobley CM, Zeng J, Sun Y, Xia Y (2009) Synthesis of anatase TiO₂ nanocrystals with exposed {001}. *Facets Nano Lett* 9:2455–2459. doi:10.1021/nl901181n
- Deng ZW, Chen M, Gu GX, Wu LM (2008) A facile method to fabricate ZnO hollow spheres and their photocatalytic property. *J Phys Chem B* 112:16–22
- Dinkar V, Shridhar S, Madhukar E, Anil E, Nitin H (2016) Sm-doped TiO₂ nanoparticles with high photocatalytic activity for ARS dye under visible light synthesized by ultrasonic assisted Sol-gel method oriental. *Journal of Chemistry* 32: 933–940. doi:10.13005/ojc/320219
- Escard J, Mavel G, Guerschais JE, Kergoat R (2002) X-ray photoelectron spectroscopy study of some metal(II) halide and Pseudohalide complexes. *Inorg Chem* 13:695–701
- Froschl T et al (2012) High surface area crystalline titanium dioxide: potential and limits in electrochemical energy storage and catalysis. *Chem Soc Rev* 41:5313–5360
- Gao CM et al (2008) Luminescence enhancement in bromine and samarium co-doped TiO₂ semiconductor nanocrystalline powders. *J Lumin* 128:559–564
- Hashimoto K, Irie H, Fujishima A (2005) TiO₂ photocatalysis: a historical overview and future prospects. *Jpn J Appl Phys* 1(44):8269–8285
- Hong XT et al (2005) Visible-light-activated nanoparticle photocatalyst of iodine-doped titanium dioxide. *Chem Mater* 17:1548–1552
- Irie H, Watanabe Y, Hashimoto K (2003) Carbon-doped anatase TiO₂ powders as a visible-light sensitive photocatalyst. *Chem Lett* 32:772–773
- Kamada M, Aita O, Ichikawa K, Okusawa M, Tsutsumi K (1992) Photoelectron spectroscopic study of the decay process of excited 4d states in cesium halides. *Phys Rev B* 45:12725–12729. doi:10.1103/PhysRevB.45.12725
- Kamada M, Ichikawa K, Aita O (1993) Solid-state effects on nonradiative decay of 4d94f1 states in barium halides. *Phys Rev B* 47:3511–3516. doi:10.1103/PhysRevB.47.3511
- Kesong Yang YD, Huang B, Whangbo M-H (2009) Density functional characterization of the visible-light absorption in substitutional C-anion- and C-cation-doped TiO₂. *Journal of Physical Chemistry C* 113:2624–2629
- Klosek S, Raftery D (2001) Visible light driven V-doped TiO₂ photocatalyst and its photooxidation of ethanol. *J Phys Chem B* 105:2815–2819
- Kumar SG, Devi LG (2011) Review on modified TiO₂ photocatalysis under UV/visible light: selected results and related mechanisms on interfacial charge carrier transfer dynamics. *J Phys Chem A* 115:13211–13241

- Kuo CY, Hsiao HM (2015) Preparation of iodine doped titanium dioxide to photodegrade aqueous bisphenol a under visible light. *Process Saf Environ* 95:265–270
- Li J, Li F, Xu Z, Zhuang Y, Zhang S (2015) Nonlinear I–V behavior in colossal permittivity ceramic:(Nb + In)co-doped rutile TiO₂. *Ceram Int* 41:S798–S803. doi:10.1016/j.ceramint.2015.03.156
- Liu G, Chen ZG, Dong CL, Zhao YN, Li F, Lu GQ, Cheng HM (2006) Visible light photocatalyst: iodine-doped mesoporous titania with a bicrystalline framework. *J Phys Chem B* 110:20823–20828
- Liu G et al (2009) Iodine doped anatase TiO₂ photocatalyst with ultra-long visible light response: correlation between geometric/electronic structures and mechanisms. *J Mater Chem* 19:2822–2829
- Liu G, Sun C, Smith SC, Wang L, Lu GQ, Cheng H-M (2010) Sulfur doped anatase TiO₂ single crystals with a high percentage of {001} facets. *J Colloid Interf Sci* 349:477–483
- Liu Y, Xie CS, Li J, Zou T, Zeng DW (2012) New insights into the relationship between photocatalytic activity and photocurrent of TiO₂/WO₃ nanocomposite. *Appl Catal a-Gen* 433:81–87
- Lou XW, Archer LA, Yang ZC (2008) Hollow micro-/nanostructures: synthesis and applications. *Adv Mater* 20:3987–4019. doi:10.1002/adma.200800854
- Luo H, Takata T, Lee Y, Zhao J, Domen K, Yan Y (2004) Photocatalytic activity enhancing for titanium dioxide by Co-doping with bromine and chlorine. *Chem Mater* 16:846–849. doi:10.1021/cm035090w
- Ohno T, Mitsui T, Matsumura M (2003) Photocatalytic activity of S-doped TiO₂ photocatalyst under visible light. *Chem Lett* 32:364–365
- Setvin M et al (2013) Reaction of O₂ with subsurface oxygen vacancies on TiO₂ anatase (101). *Science* 341:988–991
- Shen WH, Zhu YF, Dong XP, Gu JL, Shi JL (2005) A new strategy to synthesize TiO₂-hollow spheres using carbon spheres as template. *Chem Lett* 34:840–841
- Shen Y, Xiong T, Du H, Jin H, Shang J, Yang K (2009) Investigation of Br–N Co-doped TiO₂ photocatalysts: preparation and photocatalytic activities under visible light. *J Sol-Gel Sci Techn* 52:41–48. doi:10.1007/s10971-009-2007-1
- Sheng YG, Xu Y, Jiang D, Liang LP, Wu D, Sun YH (2008) Hydrothermal preparation of visible-light-driven N-Br-codoped TiO(2) photocatalysts. *Int J Photoenergy*
- Song H, Li Y, Lou Z, Xiao M, Hu L, Ye Z, Zhu L (2015a) Synthesis of Fe-doped WO₃ nanostructures with high visible-light-driven photocatalytic activities. *Appl Catal B Environ* 166-167:112–120. doi:10.1016/j.apcatb.2014.11.020
- Song H, Li YG, Lou ZR, Xiao M, Hu L, Ye ZZ, Zhu LP (2015b) Synthesis of Fe-doped WO₃ nanostructures with high visible-light-driven photocatalytic activities. *Appl Catal B-Environ* 166:112–120
- Sun XM, Li YD (2004) Colloidal carbon spheres and their core/shell structures with noble-metal nanoparticles *Angew. Chem Int Edit* 43:597–601
- Tojo S, Tachikawa T, Fujitsuka M, Majima T (2008) Iodine-doped TiO₂ photocatalysts: correlation between band structure and mechanism. *J Phys Chem C* 112:14948–14954
- Tong TZ, Zhang JL, Tian BZ, Chen F, He DN (2008) Preparation of Fe(3+)-doped TiO(2) catalysts by controlled hydrolysis of titanium alkoxide and study on their photocatalytic activity for methyl orange degradation. *J Hazard Mater* 155:572–579
- Toshiaki Ohsaka FI, Fujiki Y (1978) Raman Spectrum of anatase, TiO₂. *Journal of Raman Spectroscopy* 7:321–324
- Wang H, Lewis JP (2006) Second-generation photocatalytic materials: anion-doped TiO₂. *J Phys-Condens Mat* 18:421–434
- Wang CH, Chu XF, Wu MM (2007) Highly sensitive gas sensors based on hollow SnO₂ spheres prepared by carbon sphere template method. *Sensor Actuat B-Chem* 120:508–513
- Wetchakun N, Phanichphant S (2008) Effect of temperature on the degree of anatase-rutile transformation in titanium dioxide nanoparticles synthesized by the modified sol-gel method. *Curr Appl Phys* 8:343–346
- Wu HB, Hng HH, Lou XW (2012) Direct synthesis of anatase TiO₂ nanowires with enhanced photocatalytic activity. *Adv Mater* 24:2567–2571
- Xu AW, Gao Y, Liu HQ (2002) The preparation, characterization, and their photocatalytic activities of rare-earth-doped TiO₂ nanoparticles. *J Catal* 207:151–157
- Xu L et al (2009) ZnO with different morphologies synthesized by Solvothermal methods for enhanced photocatalytic activity. *Chem Mater* 21:2875–2885. doi:10.1021/cm900608d
- Xu H, Ouyang S, Li P, Kako T, Ye J (2013) High-active anatase TiO(2) nanosheets exposed with 95% {100} facets toward efficient H(2) evolution and CO(2) photo-reduction. *ACS Appl Mater Interfaces* 5:1348–1354. doi:10.1021/am302631b
- Xu H, Ouyang S, Liu L, Wang D, Kako T, Ye J (2014) Porous-structured Cu₂O/TiO₂ nanojunction material toward efficient CO₂ photoreduction. *Nanotechnology* 25:165402. doi:10.1088/0957-4484/25/16/165402
- Yang HG et al (2008a) Anatase TiO₂ single crystals with a large percentage of reactive facets. *Nature* 453:638–641
- Yang KS, Dai Y, Huang BB, Whangbo MH (2008b) Density functional characterization of the band edges, the band gap states, and the preferred doping sites of halogen-doped TiO₂. *Chem Mater* 20:6528–6534
- Yu JQ, Kudo A (2006) Effects of structural variation on the photocatalytic performance of hydrothermally synthesized BiVO₄. *Adv Funct Mater* 16:2163–2169
- Yu JC, Yu JG, Ho WK, Jiang ZT, Zhang LZ (2002) Effects of F-doping on the photocatalytic activity and microstructures of nanocrystalline TiO₂ powders. *Chem Mater* 14:3808–3816
- Yu JG, Liu SW, Yu HG (2007) Microstructures and photoactivity of mesoporous anatase hollow microspheres fabricated by fluoride-mediated self-transformation. *J Catal* 249:59–66
- Yu JG, Yu XX, Huang BB, Zhang XY, Dai Y (2009) Hydrothermal synthesis and visible-light photocatalytic activity of novel cage-like ferric oxide hollow spheres. *Cryst Growth Des* 9:1474–1480. doi:10.1021/cg800941d
- Zhang P, Shao CL, Zhang ZY, Zhang MY, Mu JB, Guo ZC, Liu YC (2011a) TiO₂@carbon core/shell nanofibers: controllable preparation and enhanced visible photocatalytic properties. *Nanoscale* 3:2943–2949
- Zhang Q, Li Y, Ackerman EA, Gajdardziska-Josifovska M, Li H (2011b) Visible light responsive iodine-doped TiO₂ for photocatalytic reduction of CO₂ to fuels. *Appl Catal A Gen* 400:195–202. doi:10.1016/j.apcata.2011.04.032
- Zhang Q, Gao T, Andino JM, Li Y (2012) Copper and iodine co-modified TiO₂ nanoparticles for improved activity of CO₂ photoreduction with water vapor. *Appl Catal B Environ* 123-124:257–264. doi:10.1016/j.apcatb.2012.04.035

- Zhang Y et al (2015) C-doped hollow TiO₂ spheres: in situ synthesis, controlled shell thickness, and superior visible-light photocatalytic activity. *Appl Catal B-Environ* 165: 715–722
- Zhao W, Feng LL, Yang R, Zheng J, Li XG (2011) Synthesis, characterization, and photocatalytic properties of Ag modified hollow SiO₂/TiO₂ hybrid microspheres. *Appl Catal B-Environ* 103:181–189
- Zhou JK, Lv L, Yu JQ, Li HL, Guo PZ, Sun H, Zhao XS (2008) Synthesis of self-organized polycrystalline F-doped TiO₂ hollow microspheres and their photocatalytic activity under visible light. *J Phys Chem C* 112:5316–5321